



저작자표시-비영리-변경금지 2.0 대한민국

이용자는 아래의 조건을 따르는 경우에 한하여 자유롭게

- 이 저작물을 복제, 배포, 전송, 전시, 공연 및 방송할 수 있습니다.

다음과 같은 조건을 따라야 합니다:



저작자표시. 귀하는 원저작자를 표시하여야 합니다.



비영리. 귀하는 이 저작물을 영리 목적으로 이용할 수 없습니다.



변경금지. 귀하는 이 저작물을 개작, 변형 또는 가공할 수 없습니다.

- 귀하는, 이 저작물의 재이용이나 배포의 경우, 이 저작물에 적용된 이용허락조건을 명확하게 나타내어야 합니다.
- 저작권자로부터 별도의 허가를 받으면 이러한 조건들은 적용되지 않습니다.

저작권법에 따른 이용자의 권리는 위의 내용에 의하여 영향을 받지 않습니다.

이것은 [이용허락규약\(Legal Code\)](#)을 이해하기 쉽게 요약한 것입니다.

[Disclaimer](#)

Thesis for the Degree of Master of Engineering

**Photoacoustic microscopy diagnostic
modality: an advanced system based on
high power laser diode**



by

Van Tu Nguyen

Department of Biomedical Engineering

The Graduate School

Pukyong National University

August 2017

**Photoacoustic microscopy diagnostic modality: an
advanced system based on high power laser diode**

(광음향 진단법- 고출력 레이저 다이오드

현미경 기반 고급 시스템)

Advisor: Prof. Junghwan Oh

by

Van Tu Nguyen

**A thesis submitted in partial fulfillment of the requirements
for the degree of**

Master of Engineering

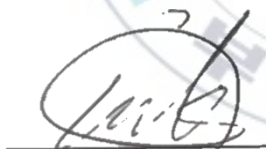
**in Department of Biomedical Engineering, The Graduate School,
Pukyong National University**

August 2017

Photoacoustic microscopy diagnostic modality: an advanced system based on high power laser diode

A dissertation
by
Van Tu Nguyen

Approved by:



(Chairman) YongWook Lee



(Member) Hyun-Wook Kang



(Member) Junghwan Oh

August 2017

LIST OF CONTENTS

Abstract.....	iii
List of Figures.....	v
List of Tables	viii
Chapter 1. Introduction	1
1.1 The fundamental of photoacoustic imaging.....	1
1.2 High-power laser diode photoacoustic microscopy system	6
Chapter 2. Materials and Methods	10
2.1 Transmission Mode Photoacoustic Microscopy	11
2.2 Reflection Mode Photoacoustic Microscopy	12
2.3 Phantom preparation	14
2.4 Ex vivo experiment	15
2.5 In vivo experiment	15
Chapter 3. Results	17
3.1 Transmission mode photoacoustic microscopy	17
3.2 Reflection mode photoacoustic microscopy	25
Chapter 4. Discussion.....	30
Chapter 5. Conclusion.....	33

References 34

Acknowledgement..... 37



Photoacoustic microscopy diagnostic modality: an advanced system based on high power laser diode

Van Tu Nguyen

Department of Biomedical Engineering,
The Graduate School, Pukyong National University

Abstract

Photoacoustic microscopy (PAM) is an efficient, noninvasive and three-dimensional imaging modality capable of imaging organs, tissues, and cellular structures with high resolution. However, the popularity of the PAM systems generally used are inconvenient and expensive solid-state laser source. Therefore, a cost-efficient and compact PAM system using the high power pulsed laser diode (PLD) has been used to develop its advantages in biological applications. In this study, two significantly improvement configuration PAM of using PLD is presented. A low loss microscopy objective lens is used to persist the laser power which set up two PAM systems: transmission mode (TM) and reflection mode (RM) PAM. The commercial focused transducer with central frequency of 5 MHz is employed to pick up the photoacoustic (PA) signal which were rebuilt to 2D images via MATLAB software. The lateral resolution of two PAM systems can be estimated to $\sim 40 \mu\text{m}$ by imaging carbon fiber. On the other hand, we imaged the phantom, *ex vivo*, *in vivo* with poly-pyrrole methylene blue nanoparticles (PPy-MB NPs) as a contrast agent to evaluate the productivity of our PAM systems. Moreover, we also perform *in vivo* mouse ear experiment to further demonstrated the feasibility of using high power PLD for PAM systems. The results of these experiments suggest that our PLD PAM system is potential for developing of photoacoustic imaging tool.

Keywords: Photoacoustic imaging, transmission mode PAM, reflection mode PAM, ultrasound imaging, nanoparticles contrast agent, 2D reconstruction.



List of Figures

Figure 1.1. The illustration of basic principle of the photoacoustic effect.	5
Figure 1.3. The absorption spectrum of PPy MB NPs.....	9
Figure 2.1. The configuration of transmission mode PAM system. LD, laser diode; CL, collimated lens; WT, water tank, TG, target; OL, microscopy objective lens, AW. Acoustic window; UT: Ultrasound transducer.	12
Figure 2.3. The configuration of reflection mode PAM system. OM, off axis mirror; AL: Aspheric lens; CL2, correcting lens; UG, ultrasound gel; M. mirror (reflected PA signal but transmitted the laser beam)	13
Figure 3.1. Photoacoustic image of carbon fiber a) PA image of carbon fiber and b) image intensity profile across the PA image, along the dashed line.	18
Figure 3.2. The TM PAM with PPy-MB NPs contrast agent. a) The FESEM of PPy-MB NPs, b) The UV-Vis absorption of PPy-MB NPs, c) Photo and PA image with the ROI of PPy-MB NPs phantom (The concentration of four samples is correspondingly 500, 250, 125, and 0 [unit: $\mu\text{g/ml}$] from the left to the right), and d) Plot	

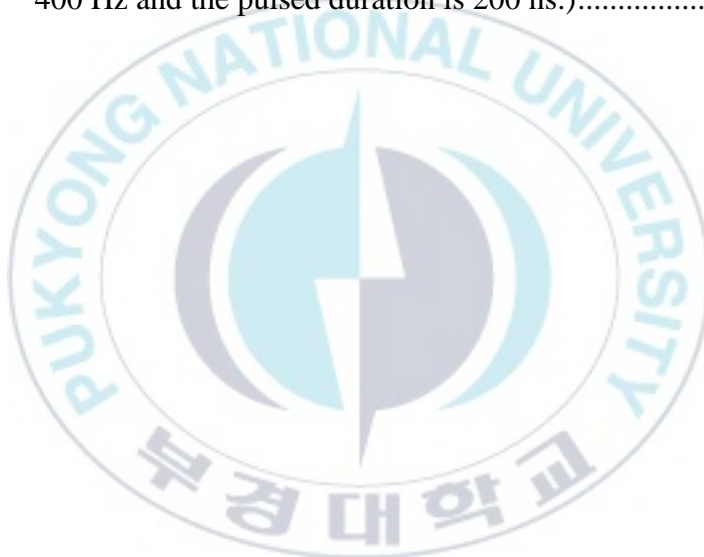
of the photoacoustic amplitude as a function of PPy-MB NPs solution concentration.....	21
Figure 3.3. The ex vivo results with the porcine liver tissue. a) Photo of porcine liver tissue, b) Photo of porcine liver tissue after injecting 10 μ l PPy-MB NPs (Concentration: 250 μ g/ml), c) The ROI liver with the size of 11 \times 11 mm ² for imaging, d) PA MAP image of porcine liver tissue.	22
Figure 3.4. The in vivo experiment results of the TM PAM system. a) Photo of the mouse ear, b) the ROI of the mouse ear 12 x 4 mm ² , c) PA MAP image of the mouse ear.	24
Figure 3.5. Photoacoustic image of a single carbon fiber a) PA image of carbon fiber and b) image intensity profile across the PA image, along the dashed line.	26
Figure 3.6. The in vivo results with the liver tissue with PPy-MB NPs contrast agent. a) Photo of the back of mouse after subcutaneously injecting 10 μ l (250 μ l/ml) PPy-MB NPs; b) The area of the PPY-MB NPs injected skin from PA MAP image in (c); c) Sequential PA PAM image of the ROI captured at 15, 30, 45, 60, 75, 90, 105, 120, 135, and 150 mins respectively. Area of the ROI is 5 \times 5 mm ²	27

Figure 3.7. The in vivo experiment results with the mouse ear of reflection
mode PAM. a) Photo of the mouse ear with the ROI for imaging;
b) PA MAP imaging of the mouse ear..... 28



List of Tables

Table 1. Optical and acoustic values for biological tissues and popular media.....	3
Table 2. Comparison between input, output energy of different microscopy objective lens to focus the PLD (Operates with the frequency 400 Hz and the pulsed duration is 200 ns.).....	11



Chapter 1. Introduction

1.1 The fundamental of photoacoustic imaging

Photoacoustic (PA) technique was discovered in 1880 by Alexander Graham bell, when he was doing experiment with long-distance sound transmission [1]. Thereafter, until the laser was developed in the 1960s with high power, directionality and coherent light, the development of many PA sensing applications was necessary. In the 1970s and 1980s, PA sensing application was beginning to use in industrial and scientific. However, PA application generally used indirectly by laser-induced surface heating of gas-phase cell type, where PA signals propagating in a gas was detected with a microphone [2]. Until the mid-1990s, PA started to be applied in biomedical imaging and the first images began to come out. Then, in the early to mid-2000s, the first PA images *in vivo* was acquired. From this time, PA technical was growth rapidly in terms of developing of instrumentation, image reconstruction algorithms, functional and molecular imaging capabilities in clinical research.

Photoacoustic imaging (PAI) is formed on the photoacoustic effects which is the formation of ultrasound waves according to the absorption of the light (mostly short pulses laser light) and generates heat excitation in a

material sample. The absorption of the pulsed laser light in a biological tissue could be simulated by the Beer-Lambert law:

$$I = I_0 e^{-\mu_a L} \quad (1.1)$$

where, I is the light intensity after traveling L meters, I_0 is the initial intensity of the light and μ_a is the optical absorption coefficient of the tissue [3].

In this modality, a few nanosecond pulse widths laser is mostly used to illuminating the biological tissues. Due to the fact that, to generate wideband ultrasonic emission in the samples, the laser pulses have to be smaller than both the thermal relaxation time (τ_{th}) and the stress relaxation time (τ_s):

$$\tau_{th} = \frac{d_c^2}{\alpha_{th}} \quad (1.2)$$

$$\tau_s = \frac{d_c}{v_s} \quad (1.3)$$

of the biological tissues; where, d_c is the size of the interest object, α_{th} is the thermal diffusivity of the tissue, and v_s is the sound velocity in the tissue [3]. Table 1.1 shows the values of optical absorption coefficient, thermal diffusivity and sound velocity for some biological tissues and popular media[4, 5].

In photoacoustic imaging, some of the transported laser light will be absorbed and converted into heat, ultrasound waves can be emitted within the irradiated area due to the short thermos-elastic expansion of the tissues. These ultrasound waves can be detected and picked up to produce a photoacoustic image by an ultrasound transducer. As a result, the amplitude of the ultrasound waves (i.e. photoacoustic signal), which is proportional to the local energy deposition, disclose physiologically specific optical absorption contrast. Therefore, PAI effectively combines the contrast of optical imaging techniques with the penetration depth and the resolution of ultrasound imaging [3, 6-10]. The schematic diagram of the fundamental photoacoustic effect is shown in Figure 1.1. Short laser pulses are employed to irradiate in the sample. A part of laser energy is absorbed by the sample and it is converted into ultrasound waves by thermo-elastic phenomenon, which consequently leads to ultrasonic emission. The photoacoustic signals are gathered by the ultrasonic detector to build images. The image reconstruct algorithms is applied to form 2D and 3D photoacoustic image. For acoustic coupling, the liquid such as water which have elastic medium is used for propagating ultrasound waves.

Table 1. Optical and acoustic values for biological tissues and popular media.

Tissue/Media	Absorption coefficient (cm^{-1}) ^a	Sound velocity (m.s^{-1}) ^b	Thermal diffusivity ($\text{mm}^2.\text{s}^{-1}$) ^b
Air	-	344	19
Fat	0.7	1450	0.045
Muscle	-	1584	0.16
Brain tissue	1.6	1558	0.13
Blood	1.3	1570	0.13
Bones	-	4080	0.39
Liver	2.3	1570	0.15
Kidney	-	1560	0.15
Epidermis	1.5	1645	0.09
Dermis	2.7	1595	-
Water	-	1480	23.38

^a Parameters for 633-635 nm *in vitro*.

^b Parameters at room temperature.

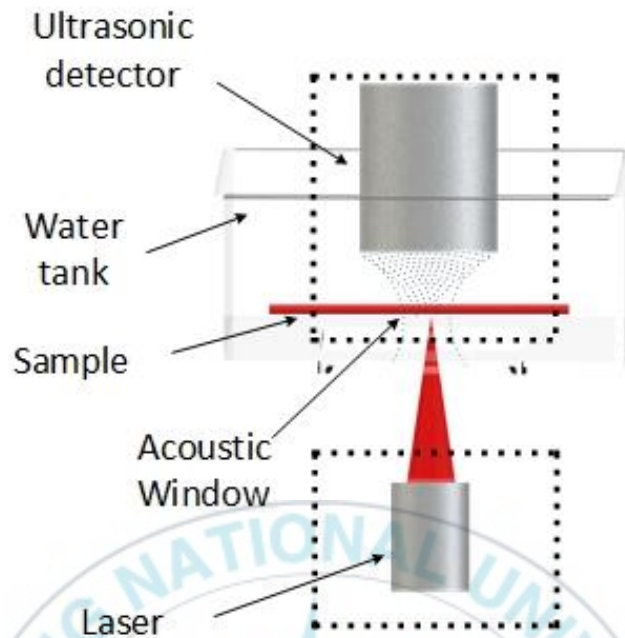


Figure 1.1. The illustration of basic principle of the photoacoustic effect.

For more details, in PA imaging, laser wavelengths in the visible and near-infrared (NIR) ranges (500- 900 nm) are most typically employed. The NIR range from 600-900 nm provide the biggest penetration depth widen to several centimeters. If PA imaging uses the microwave band from 300 MHz to 3 GHz, it can offer better penetration depths. In this excitation of light, each tissue such as hemoglobin, melanin, or waters have a specific absorption coefficient impinges by rapid heat generate a little temperature changes (approx. smaller than 0.1 K). It might be cause the physical damage or change the properties of tissues. The reason is that increasing the initial pressure, then emitted the broadband with low magnitude of ultrasound

waves. They are detecting by either a single transducer scanner or an array of ultrasound detectors to collect a serial of A-lines. Based on the speed of sound and time of propagation of ultrasound waves, the photoacoustic can be form by the same algorithms of the conventional pulse-echo ultrasound image.

1.2 High-power laser diode photoacoustic microscopy system

Photoacoustic imaging (PAI) is an efficient, noninvasive and three-dimensional imaging modality capable of imaging organs, tissues, and cellular structures with high resolution. It combines the benefits of both optical and acoustic imaging [11]. Since the last decade, researchers have witnessed a significant progress in PAI. The substantial contribution of PAI helps to the development of diagnostic instruments to detect the brain structure and function [12], vasculature networks [13], organic cells [14], heterogeneous media [15], chemical traces [16], and tumor tissue [17]. A short-pulsed laser source is used for tissue irradiation and a transducer is employed to collect the photoacoustic signals created by the thermo-elastic expansion phenomenon [18], [19]. Photoacoustic microscopy is an important branch of the photoacoustic imaging system in terms of the high spatial resolution, image contrast, and depth penetration. PAM supplies high sensitivity to optical absorption and opens a new strategy to study

biological systems in terms of multiple length and timescales [20]. It has great potential for biological tissue imaging in tissue and for resolving blood vessels with much higher spatial resolution than the present photoacoustic imaging with ultrasound array transducers [21], [22]. Especially, optical resolution and acoustic resolution photoacoustic microscopy are key mapping vasculature networks in clinical biological application [23]. In addition, PAT using exogenous contrast agent enable the sensitivity of molecular and extremely expands the performance of the modality [24], [25], [26].

Although PAM has many advantages for biological tissue imaging, the popularity of the PAM systems generally used are bulky and expensive laser source such as Q-switched Nd: YAG laser and optical parametric oscillator. Furthermore, the low pulse repetition frequency (about 10 Hz) is not suitable for PAM systems in clinical applications.

On the other hand, a high-power pulsed laser diode (PLD) excitation has been found as an alternative laser source. With some advantage properties: low-cost laser, compact, and high pulse repetition frequency, PLD could overcome those limitations to grow its application. In addition, PLDs are available with a wide range of visible and (NIR) wavelengths without supplement components. In consequence, a PAM model system using the high-power PLD may be a compact system to excite small sample

areas to have enough energy density. However, the main drawback of the high-power PLD is its long pulse duration, which hinders the efficient photoacoustic effect for the tiny vessels [21]. Furthermore, the high power PLDs with multiple active elements are paid off by the intrinsic anisotropy of the beam which is a remarkable challenge to achieving a low-loss focusing of light, thus hindering the high-power PLD in applications of PAM systems [27], [28], [29]. In this study, an upgraded PAM system is introduced by using a high-power laser diode excitation. According to the previous literature [30], [31], two different PLD-PAI configurations: TM PAM and RM PAM were built. A microscope objective lens with low-loss light energy was used to focus the divergent beam to maintain the energy power in the TM PAM. Whereas, for RM PAM, an off-axis mirror is used to collimate the focused light to obtain the high field of view (FOV) for biomedical imaging applications. In order to demonstrate our productivity of PAM systems, we present the results of imaging ex vivo of porcine liver tissue, and in vivo of the mouse ear. Particularly, the PPy-MB NPs are used as exogenous nanomaterials to trace its biodistribution and transportation in biological systems. Figure 1.3 show the absorption spectrum of PPy-MB NPs with strongly absorbing of the NIR range. With good absorption in NIR range, the penetration depth of our PAM system is optimized. The

experimental results suggest the feasibility of the laser diode of both PAM systems for future producibility.

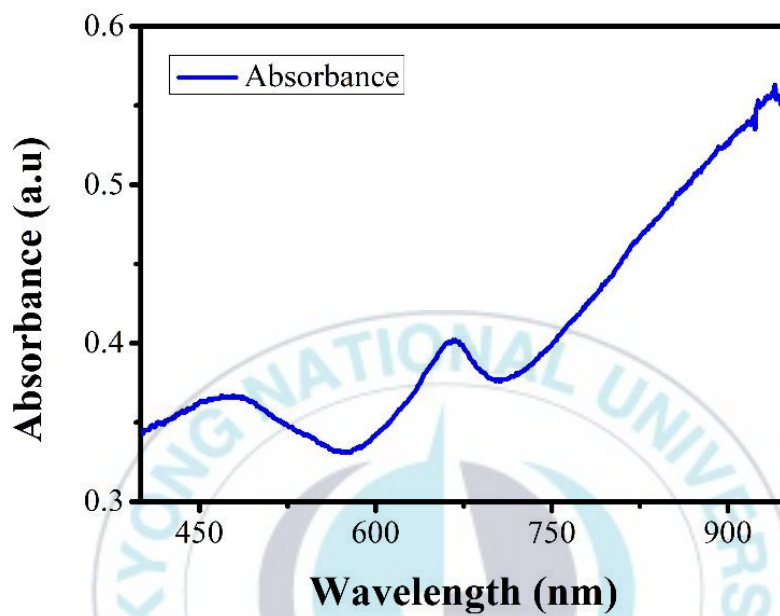


Figure 1.2. The absorption spectrum of PPy MB NPs.

Chapter 2. Materials and Methods

A high power PLD (Laser Components, 905D5S2L3J08S) was applied as a substitute excitation source. The stacked arrays with 10 active elements of PLD generated the emitting area of $800 \times 440 \mu\text{m}^2$. The divergence of each slow and fast axis was 10° and 25° , respectively. This is the reason for an extreme limitation in collimation and focusing of the laser light [27-29]. To deal with this limitation, an aspheric lens (Thorlabs, 354330-B) was chosen as the first element with sufficiently high NA ($f = 3.1 \text{ mm}$, $\text{NA} = 0.68$, AR coated for 600-1050 nm) to collect the divergent beam without losing the laser light. The aspheric was attached to the collimation tube (Thorlabs, LTN330-B). Then, to get optical resolution, a microscopy optical lens is employed. According to the literature, the current microscope lens significantly losses energy [29]. Another study illustrates, a low-loss microscope objective lens (Plan 40X, $\text{NA} = 0.65$, Leica, Japan) with anisotropic beam. In Table 1.2, a comparison between input, output energy of different microscope objective lenses to focus the PLD was tested. We used the Ophir sensor (PD300-3W-V1 ROHS) to measure the NIR laser light. Input energy was measured after the aspheric lens, and output energy was measured at the sample. It can be seen that the microscope objective lens of Leica (Plan 40X/0.65) transmitted nearly 66% of the 905-nm laser

light. In contrast, the microscopy objective lens of Meiji, results a total energy loss about 95.23%. Thus, the Plan 40X/0.65 Leica is one of the effective solutions to achieve the microscopy resolution without significantly losing energy. A commercial driver (PicoLAS, LDP-V 240-100 V3) helps the high power PLD to radiate the stable laser light at a 905 ± 15 nm of wavelength. The maximum peak power output of PLD is up to 650 W. In addition, a function generator (HP, 33220A) triggered the driver by the 400 Hz pulsed frequency (pulse width duration of 200 ns) and synchronized the data acquisition (NI-DAQ) board at the same time through a Transistor-Transistor-Logic trigger.

Table 2. Comparison between input, output energy of different microscopy objective lens to focus the PLD (Operates with the frequency 400 Hz and the pulsed duration is 200 ns.)

Lens	Input energy (mJ)	Output energy (mJ)	Energy loss (%)
Transmission mode S. Plan M40X 0.65 Meiji, Japan	8.4	0.4	95.23
Transmission mode Plan 40X/0.65 Leica	8.4	5.6	33.33
Reflection mode	8.4	4.8	42.86

2.1 Transmission Mode Photoacoustic Microscopy

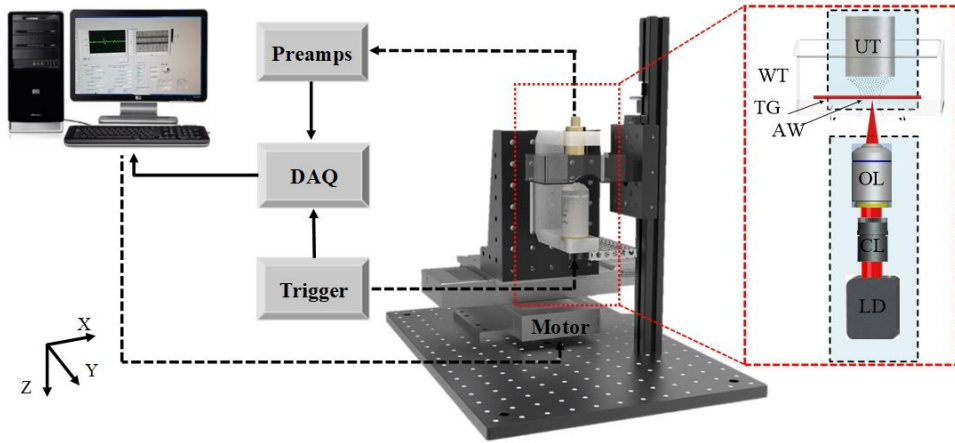


Figure 2.1. The configuration of transmission mode PAM system. LD, laser diode; CL, collimated lens; WT, water tank, TG, target; OL, microscopy objective lens, AW. Acoustic window; UT: Ultrasound transducer.

Figure 1 shows the optical resolution PAM system which is configured with TM where the laser is opposite the transducer. The photoacoustic signal is collected by the commercially focused transducer (Olympus Panametrics, NDT-V308) with a center frequency of 5 MHz. The phantom is placed on the water tank for acoustic coupling. The scanning is performed by two DC motors (Z047A, Newport, France) that move the TM PAM system in X and Y directions as raster scan (Yao and Wang 2011). In TM, the distance among microscopy objective lens, ultrasound transducer, and a sample is adjusted to achieve the maximum amplitude signal.

2.2 Reflection Mode Photoacoustic Microscopy

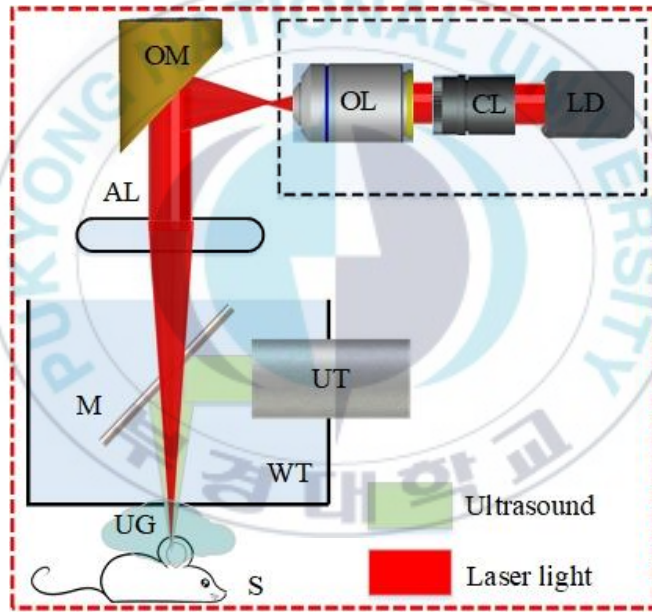
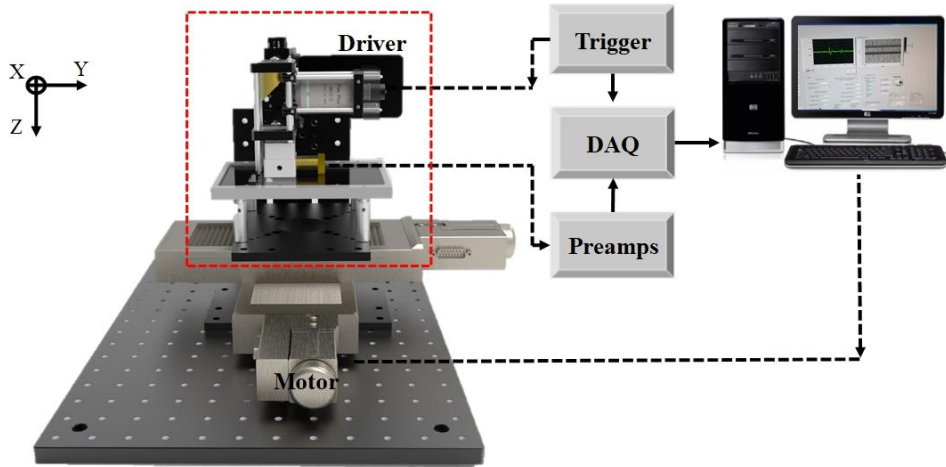


Figure 2.2. The configuration of reflection mode PAM system. OM, off axis mirror; AL: Aspheric lens; CL2, correcting lens; UG, ultrasound gel; M. mirror (reflected PA signal but transmitted the laser beam)

The reflection mode PAM is illustrated in Fig. 2. Similar to the TM PAM, the laser light in the reflection mode is focused by passing it through

the Leica microscope objective lens. Then, the focused light is placed at the focal point of an off-axis mirror (#47-096, Edmund Optics, USA), which is aligned perpendicularly with the microscope objective lens (Fig. 2). Particularly, based on the properties of the off-axis mirror, all light at the focal point is reflected about 97% and becomes parallel. An aspheric lens with focal length $f=50$ mm (#66-025, Edmund Optics, USA) was used to focus the parallel light at the sample. A commercial flat transducer 5 MHz (PAC, IU5GI) was employed to gather the photoacoustic signal. The transducer was placed perpendicularly with the laser light which as has been described [31]. The 2D raster scan is performed by smoothly moving the sample instead of moving the PAM system, which helps to reduce the load weight on DC motor.

2.3 Phantom preparation

A phantom was made by polyvinyl alcohol (PVA) that closely mimics human tissue to perform PAM experiment for checking PA signal of PPy-MB NPs. Because of some advantage properties of PVA (non-toxic, easy casting and stable storage), it is used for fabricating vessel phantom [32]. Particularly, PVA ensures good biocompatibility and, on the contrary, it lengthened the bloodstream circulation time of PPy-MB NPs [33]. PVA phantoms were made by mixing 8% PVA, 0.4% silica, and 100 mL distilled

water. Control and PPy-MB NPs were stirred with 10% gelatin and used as three additions (50 μ L each/well) in the tissue-mimicking PVA phantom. Three concentrations of PPy-MB NPs were prepared for testing the photoacoustic signal (i.e., 125 μ g/ml, 250 μ g/ml, 500 μ g/ml.)



Figure 2.4. PPy-MB NPs phantom with four different concentrations

2.4 Ex vivo experiment

For the ex vivo experiment, the porcine liver tissue was bought from a local abattoir and was stored in a refrigerator at -80 °C. Prior to the testing, the frozen sample was cut into a 3-mm thin layer and was kept in saline at 4 °C. PPy-MB NPs solution (10 μ L, 250 μ g/mL) was injected into the center of the sample for the photoacoustic imaging experiment.

2.5 In vivo experiment

Female BALB/c nude mouse and female white mouse weighing 21 g (Orient Bio Inc, Gyonggi-Do, Korea) were used for the in vivo study. In the time of experiment, the mice were kept under anesthesia with a vaporized-isoflurane system through a self-made breathing mask. The body temperature of the mice was maintained by a heating pad at 38 °C. The mice were placed on an animal bed underneath the plastic membrane. For acoustic coupling, the skin of the mice was pasted by applying degassed ultrasound gel.

We perform the in vivo experiment for the tracking PPy-MB NPs kinetics in the nude mice. A solution of PPy-MB NPs (10 μ L, 250 μ g/mL) was injected subcutaneously into the skin of the mouse. Post-injection PAM scans on the skin area were performed at 7, 30, 60, 90, 120, 150, 180 mins.

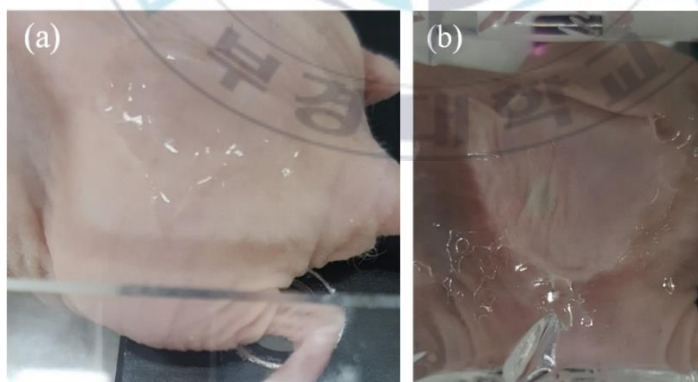


Figure 2.5. In vivo subcutaneous injection of PPy-MB NPs. (a), (b) Photo of back skin mouse before and after injection, respectively.

Chapter 3. Results

3.1 Transmission mode photoacoustic microscopy

Firstly, we imaged a single carbon fiber with $\sim 7\ \mu\text{m}$ diameter as small as capillary blood vessels to estimate the lateral resolution of our system. Figure 3a shows a maximum amplitude projection (MAP) image along the z-axis to the x-y plane of the single carbon fiber. The raster scan was performed by a motorized X-Y scanner with 400 points (for both X-Y direction) and a small step size of $2\ \mu\text{m}$. This image (Fig. 7a) was reconstructed with the small size of $0.8 \times 0.8\ \text{mm}^2$ via MATLAB software (version 8.0, Mathworks, USA). It was clear and clean with the peak signal-to-noise ratio (SNR) of the resultant PA signal about 23.28 (dB). The diameter of carbon fiber is about $7\ \mu\text{m}$. Figure 3b shows that the full half maximum width (FHMW) of the signal was about $47\ \mu\text{m}$. Therefore, the study indicates that the theoretical lateral resolution of the TM PAM system is about $40\ \mu\text{m}$.

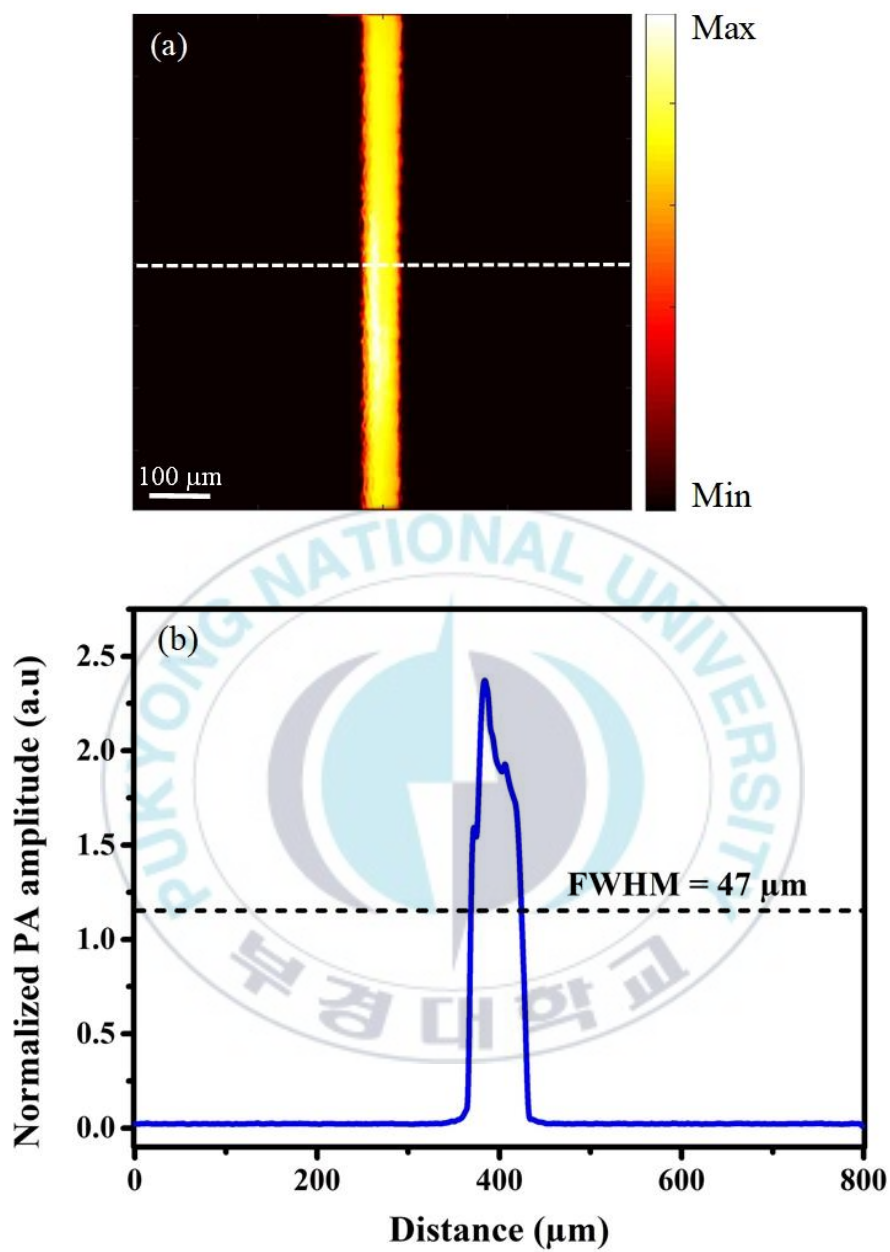
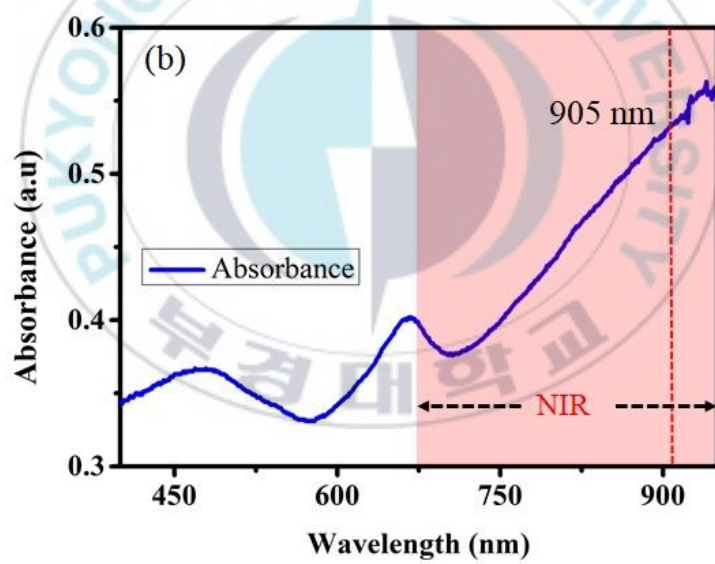
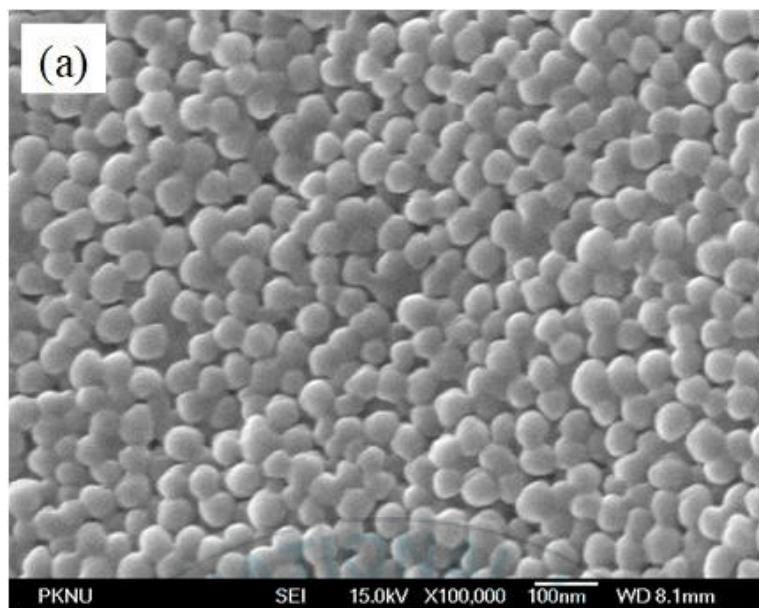


Figure 3.1. Photoacoustic image of carbon fiber a) PA image of carbon fiber and b) image intensity profile across the PA image, along the dashed line.

Secondly, in order to demonstrate the imaging ability of our PAM system, we performed the phantom experiment with polypyrrole-methylene blue nanoparticles (PPy-MB NPs) as a contrast agent. PPy-MB NPs are reported as having an excellent biocompatible, high NIR absorbance for PAT [Ref112]. Figure 4(a) shows the field emission scanning electron microscopy (FESEM) image of PPy-MB NPs. It was observed that the PPy-MB NPs are in uniform spherical morphology and the particle size is around 49.5 nm. The UV-vis-NIR spectrum of PPy-MB NPs with a high absorption of 905 nm is shown in Fig. 4b, thus 905 nm laser source is used to monitor PPy-MB NPs distribution. As shown in Fig 4c, PPy-MB NPs produced a strong photoacoustic signal when excited by the laser light at 905 nm. The scan area was 27 x 7 mm² which is along the dotted line rectangular in Fig. 4c. The PA signal intensities rose linearly with the concentrations of the PPy-MB sample (Fig. 4d). Specially, the sample with the concentration of 250 $\mu\text{g mL}^{-1}$ of PPy-MB NPs generated a strong amplitude photoacoustic. It is about fourteen times higher than control alone. Thus, the strongly absorbing PPy-MB NPs could prevail over the uncertain background solvent spectrum in the NIR region. And we chose the concentration of 250 $\mu\text{g/ml}$ of PPy-MB NPs to perform the in vivo experiment.



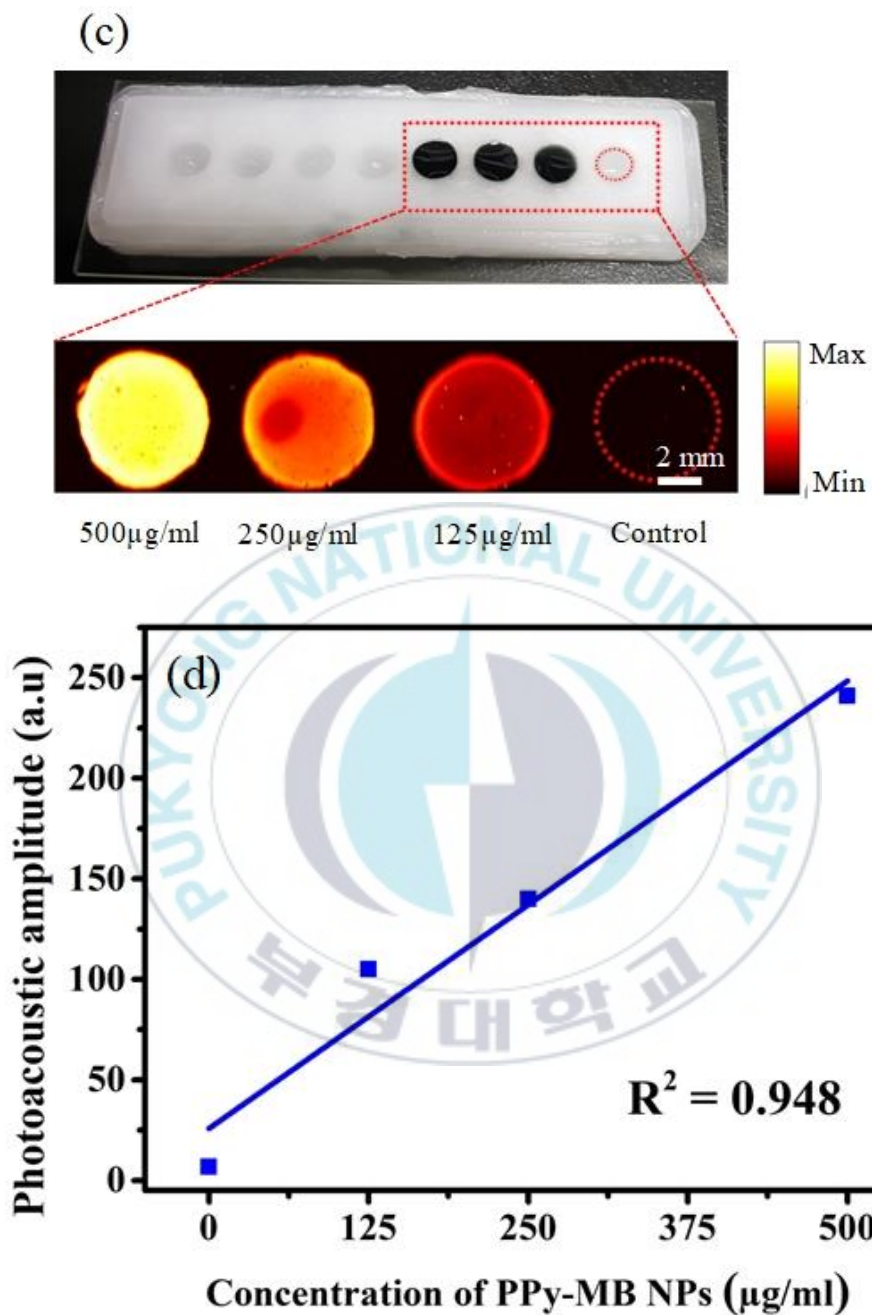


Figure 3.2. The TM PAM with PPy-MB NPs contrast agent. a) The FESEM of PPy-MB NPs, b) The UV-Vis absorption of PPy-MB NPs, c) Photo and PA image with the ROI of PPy-MB NPs phantom (The concentration of

four samples is correspondingly 500, 250, 125, and 0 [unit: $\mu\text{g/ml}$] from the left to the right), and d) Plot of the photoacoustic amplitude as a function of PPy-MB NPs solution concentration.

In contrast, the *ex vivo* experiment with the porcine liver tissue is presented in Fig. 5. We acquired PA images of 3 mm thickness porcine liver tissue (Figure 5a) injected with 10 μl PPy-MB NPs (Concentration: 250 $\mu\text{g/ml}$). Figures 5b and 5c present the ROI for imaging PA experiments with the size of $11 \times 11 \text{ mm}^2$. A PA MAP image is shown in Fig. 5d with the SNR of the image about 7.78 (dB). Its SNR is not high because the liver tissue contains a lot of blood which also generates PA signal when illuminated by laser light. However, the injected liver tissue is seen clearly compared with the photograph of porcine liver tissue.

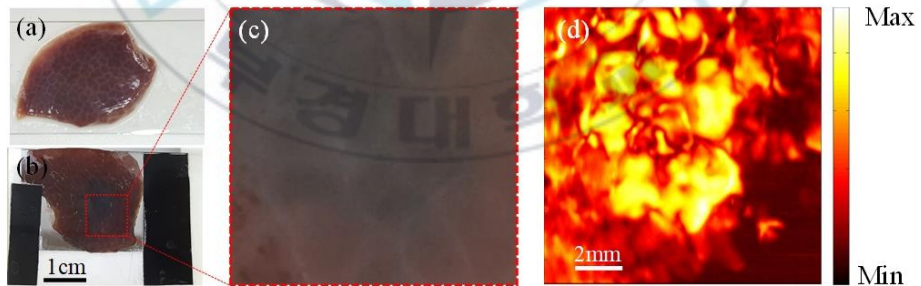


Figure 3.3. The *ex vivo* results with the porcine liver tissue. a) Photo of porcine liver tissue, b) Photo of porcine liver tissue after injecting 10 μl PPy-MB NPs (Concentration: 250 $\mu\text{g/ml}$), c) The ROI liver with the size of $11 \times 11 \text{ mm}^2$ for imaging, d) PA MAP image of porcine liver tissue.

We also imaged a nude mouse ear in vivo using TM PAM. The sample was placed on a glass (1-mm thin layer) which was white non-absorbing material. Only a part of the mouse ear was chosen to perform the experiment (red dashed rectangular in Fig. 6a) due to the limitation thickness sample of the transmission mode PAM [14], [34], [35]. The number of scanning points used in this experiment was 1,200 points (X-direction) \times 400 points (Y-direction) with a step size of 10 μm . Figures 7a and 7b are photographs of the mouse ear with the region that is captured by TM PAM. Figure 7c shows the PA image of the vasculature in the mouse ear. Particularly, the SNR of the PA signal obtained from the sample was 16.61 (dB). The time for the acquisition was about 30 min. In the reconstructed image procession, the original data was executed without any signal processing, and the linear color bar corresponds to the maximum amplitude of the photoacoustic signal which depended on the optical absorption distribution.

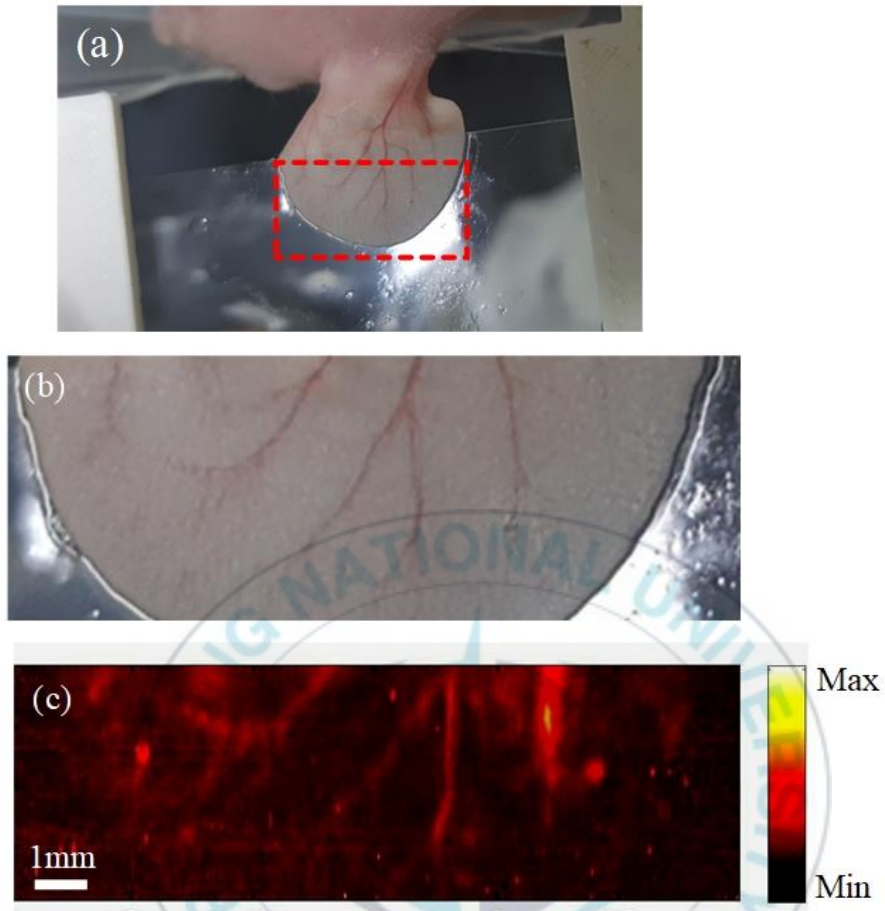
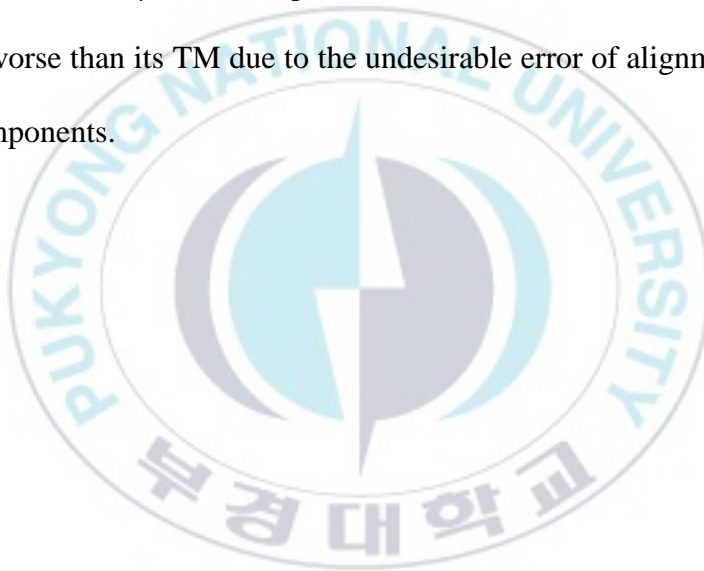


Figure 3.4. The in vivo experiment results of the TM PAM system. a) Photo of the mouse ear, b) the ROI of the mouse ear 12 x 4 mm², c) PA MAP image of the mouse ear.

3.2 Reflection mode photoacoustic microscopy

Similarly, with the TM PAM, we experimentally acquired the single carbon fiber to check the lateral resolution. In this experiment, we scanned the area with 800 points \times 800 points (for both X-Y direction) and a small step size of 2 μ m. Figure 7a shows the PA MAP image with the size of 1.6 \times 1.6 mm² and its peak SNR is 23.28 (dB), and the lateral resolution is estimated about 42 μ m. In comparison, the measured lateral resolution is slightly worse than its TM due to the undesirable error of alignment of the optic components.



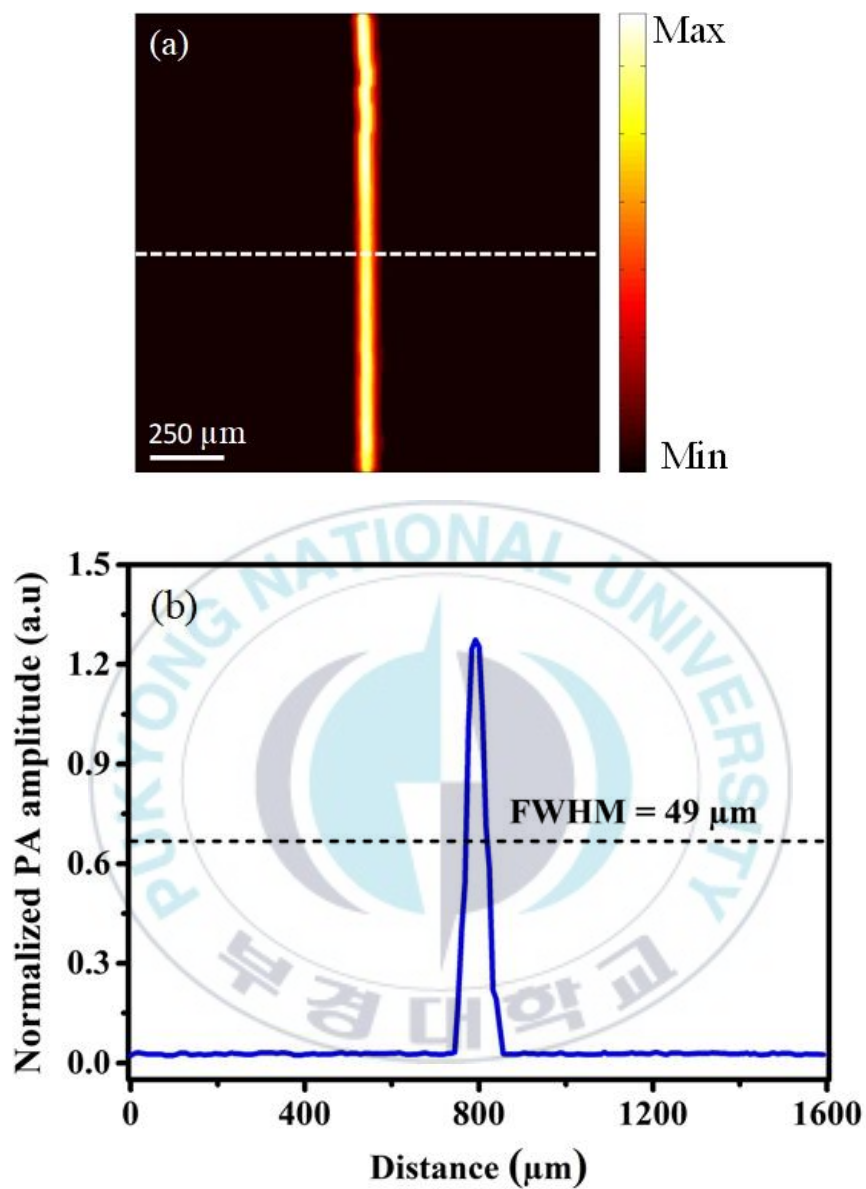


Figure 3.5. Photoacoustic image of a single carbon fiber a) PA image of carbon fiber and b) image intensity profile across the PA image, along the dashed line.

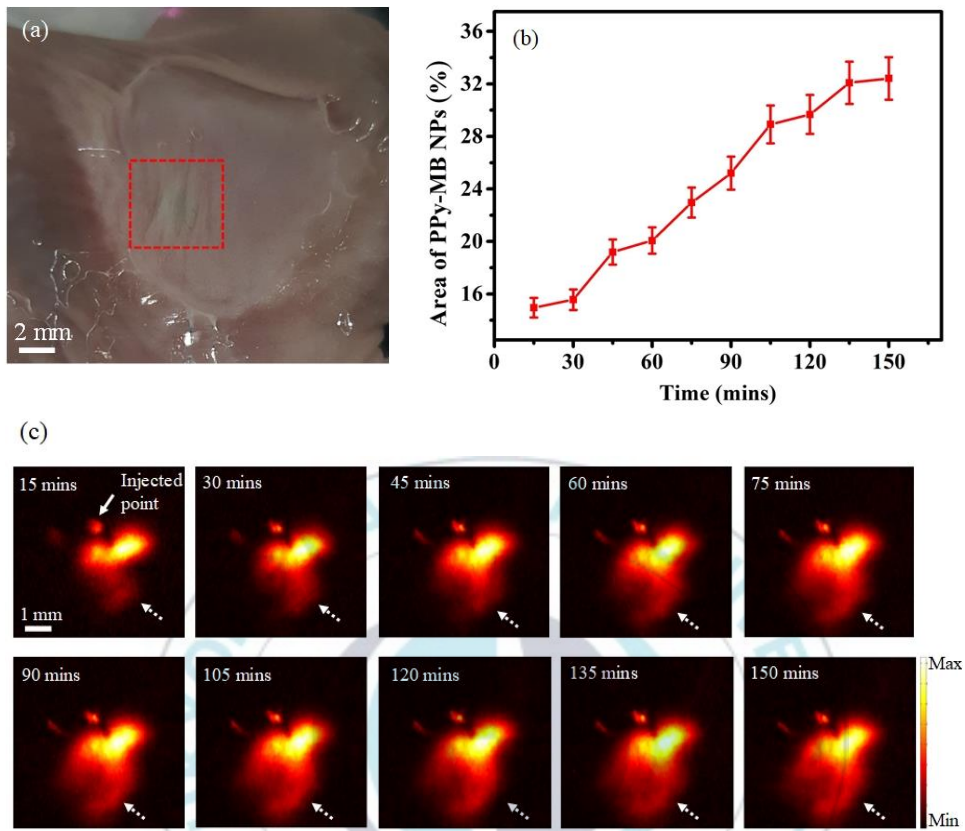


Figure 3.6. The in vivo results with the liver tissue with PPy-MB NPs contrast agent. a) Photo of the back of mouse after subcutaneously injecting 10 μ l (250 μ l/ml) PPy-MB NPs; b) The area of the PPy-MB NPs injected skin from PA MAP image in (c); c) Sequential PA PAM image of the ROI captured at 15, 30, 45, 60, 75, 90, 105, 120, 135, and 150 mins respectively. Area of the ROI is $5 \times 5 \text{ mm}^2$.

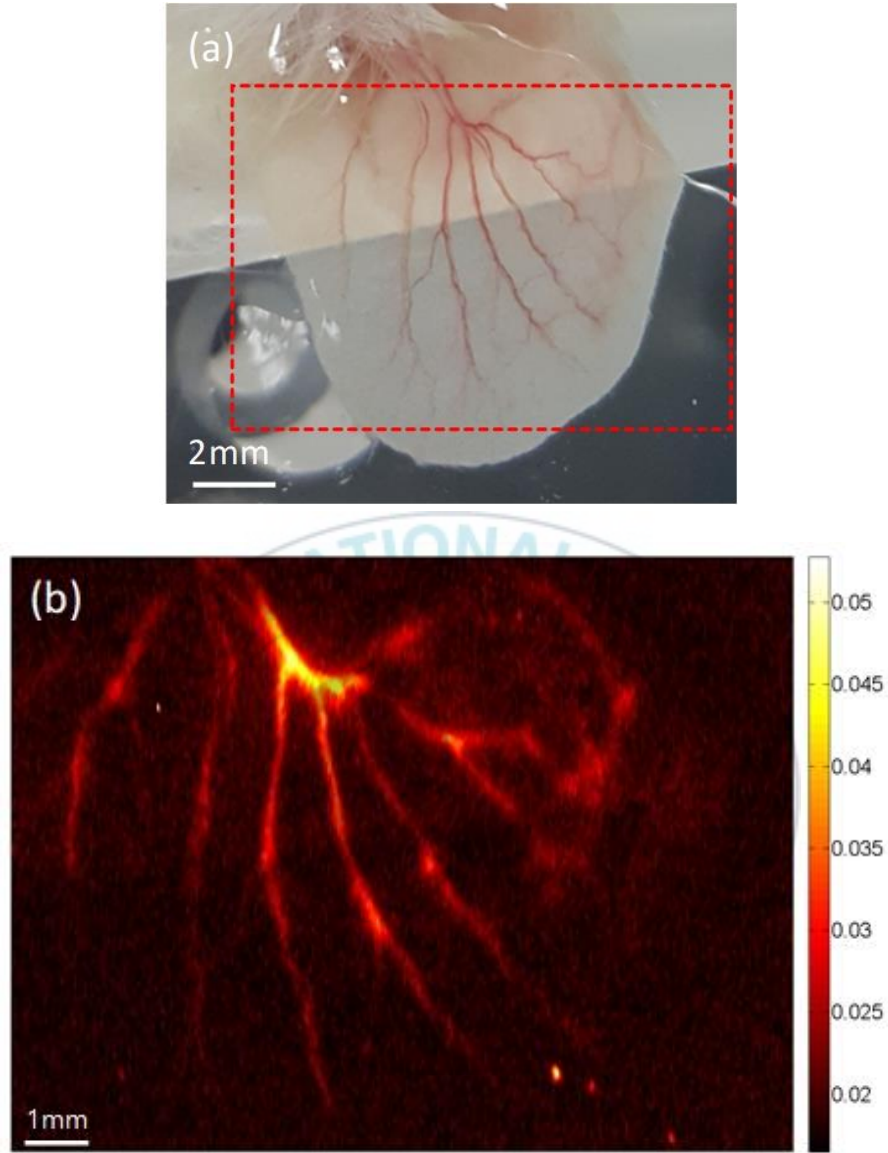


Figure 3.7. The in vivo experiment results with the mouse ear of reflection mode PAM. a) Photo of the mouse ear with the ROI for imaging; b) PA MAP imaging of the mouse ear.

To further confirm the capable results obtained from reflection mode PAM, in vivo PA image with mouse ear is collected and analyzed. After

removing the mouse skin hair, the whole ear image is captured. With the scanning size of $12 \times 9 \text{ mm}^2$, the number of points used in this experiment was 1,200 points (X-direction) and 450 points (Y-direction), corresponding with a step size of $10 \text{ }\mu\text{m}$ and $20 \text{ }\mu\text{m}$, respectively. It took about 50 min to acquire the whole of the mouse ear. The SNR of the image is 16.22 (dB). It can be seen that the vasculature of the mouse ear can be imaged clearly by the RM PAM.



Chapter 4. Discussion

We demonstrated the performance of using a high power PLD in PAI systems. Pulse width is the main limitation of most high-power light sources [27], [28], [29]. The large pulse width influences the acoustic wave generation of small vessels by limiting the stress confinement [21]. For that reason, the high-power PLD laser is not acceptable for some applications. However, with high power energy, the high SNR signal of the PAM system is feasible for imaging biological tissues. In this paper, we showed the imaging ability of two configurations of the high-power PLD PAM systems: TM PAM; and RM PAM. The PA images of several ex vivo, in vivo experiments, were presented. Several challenges were solved in this study. The intrinsic challenge of the PAM configurations was made the anisotropic beam to be collimated, then focus to the microscopy resolution. To tackle this problem, a few configurations has been mentioned in the literature [ref]. We optimized a TM configuration that uses the low loss microscopy objective lens to focus the diverging beam, then developed the reflection mode PAM with an off-axis mirror. We reported both of PAM modes; the high SNR of the PA signal was achieved, and it was slightly higher in TM. However, TM configuration has limited applications, e.g.,

imaging of a very thin sample, limiting of FOV. By contrast, the reflection mode with widened FOV is not limited by the thickness of samples. Thus, the reflection mode PAM can be an excellent tool to apply in biological applications. In reflection mode PAM configuration, the off-axis mirror is used to collimate the laser light, which solves these limitations of high-power PLD [27], [28], [29]. However, the use of more optical components in reflection mode PLD PAM is paid off by the lower SNR, and a little greater in comparison with TM PLD PAM.

The transverse resolution of PAM is calculated in theory by the formula: $0.51 \lambda / \text{NA}$ where λ is the wavelength and NA is the numerical aperture of the objective lens. The size of the spot which laser beam can be focused is proportional to the wavelength. Then, the lateral resolution of this system is about $4.6 \mu\text{m}$. However, in our PAM system, the lateral resolution is approximately 10 times more than the ideal optical diffraction limit, probably because of the extended laser emitting area of LD. In fact, we can use a micrometer level pinhole to filter the structure of the laser beam [19]. If the pinhole is small enough, we can get the very tiny spot with losing an overdone laser energy. Moreover, the laser diode irradiating the emitting area is a non-rotationally symmetric beam, which limits the collimation as well as focusing the beam of an objective lens.

In theory, the axial resolution is determined by the formula $\frac{2 \ln 2 \times c}{\pi \Delta f}$, where c is the ultrasound velocity and Δf is the bandwidth of the transducer. The axial resolution of the PAM system estimated $\sim 118 \mu\text{m}$ by 5.6 bandwidth follows the datasheet of the transducer.

In contrast, the cost of the laser diode and LD driver was only \$2.500 dollars. The size and cost of PAM have been decreased significantly. In this PAM system, after losing about 33% energy by through a group of lens, the maximum laser energy was $14 \mu\text{J}$ per pulse. At the surface phantom, the experimental energy was 5.6 mJ. This number is safe in comparison with the maximum allowed according to the safety standards of the American National Standards Institute. Therefore, our system can be applied in animal studies as well as in clinical studies in the near future.

Chapter 5. Conclusion

In summary, the feasibility of using a high-power PLD in the two configurations of PAI systems: TM PAM and RM PAM have been developed. The lateral resolution of both transmission and reflection mode PAM was experimentally calculated to be 48 μm and 51 μm respectively by imaging a single carbon fiber. The results of imaging tissue-mimicking phantoms, ear mouse vasculature and tracing PPy-MB NPs distribution indicated that the compact and efficient PAI systems will be able to set up with the high-power PLD. The remaining disadvantage of our systems is the large pulse width duration of the high power PLD, which is affected to efficient of photoacoustic imaging. In the coming work, we will concentrate on applying the laser fast scanning [36] and the combination of different laser diodes for multi-wavelength PLD PAM systems [37].

References

1. Bell, A.G., *Upon the production and reproduction of sound by light*. Journal of the Society of Telegraph Engineers, 1880. **9**(34): p. 404-426.
2. Tam, A.C., *Applications of photoacoustic sensing techniques*. Reviews of Modern Physics, 1986. **58**(2): p. 381.
3. De Montigny, E., *Photoacoustic Tomography: Principles and applications*. 2011, OCIS.
4. Fasla, B., R. Benmouna, and M. Benmouna, *On the Hyper Thermal Therapy of Tumor Tissues by Direct Laser Heating and Gold Nano Particles*. Journal of Biomaterials and Nanobiotechnology, 2014. **2014**.
5. Grossweiner, L.I., et al., *The science of phototherapy: an introduction*. 2005: Springer.
6. Sethuraman, S., et al., *Intravascular photoacoustic imaging using an IVUS imaging catheter*. Ultrasonics, Ferroelectrics and Frequency Control, IEEE Transactions on, 2007. **54**(5): p. 978-986.
7. Wang, B., et al., *Intravascular photoacoustic imaging*. Selected Topics in Quantum Electronics, IEEE Journal of, 2010. **16**(3): p. 588-599.
8. Karpouk, A.B., et al., *Feasibility of in vivo intravascular photoacoustic imaging using integrated ultrasound and photoacoustic imaging catheter*. Journal of biomedical optics, 2012. **17**(9): p. 0960081-0960086.
9. Yang, J.-M., et al., *A 2.5-mm diameter probe for photoacoustic and ultrasonic endoscopy*. Optics express, 2012. **20**(21): p. 23944-23953.
10. Bai, X., et al., *Intravascular Optical-Resolution Photoacoustic Tomography with a 1.1 mm Diameter Catheter*. PloS one, 2014. **9**(3): p. e92463.
11. Rao, B., et al., *Real-time four-dimensional optical-resolution photoacoustic microscopy with Au nanoparticle-assisted subdiffraction-limit resolution*. Optics letters, 2011. **36**(7): p. 1137-1139.
12. Wang, X., et al., *Noninvasive laser-induced photoacoustic tomography for structural and functional in vivo imaging of the brain*. Nat Biotechnol, 2003. **21**(7): p. 803-6.

13. Laufer, J., et al., *In vivo preclinical photoacoustic imaging of tumor vasculature development and therapy*. Journal of biomedical optics, 2012. **17**(5): p. 0560161-0560168.
14. Zhang, C., K. Maslov, and L.V. Wang, *Subwavelength-resolution label-free photoacoustic microscopy of optical absorption in vivo*. Optics letters, 2010. **35**(19): p. 3195-3197.
15. Yuan, Z., et al., *Finite-element-based photoacoustic tomography: phantom and chicken bone experiments*. Appl Opt, 2006. **45**(13): p. 3177-83.
16. Li, W., et al., *In vivo quantitative photoacoustic microscopy of gold nanostar kinetics in mouse organs*. Biomed Opt Express, 2014. **5**(8): p. 2679-85.
17. Li, X., et al., *High resolution functional photoacoustic tomography of breast cancer*. Med Phys, 2015. **42**(9): p. 5321-8.
18. Karabutov, A.A., et al., *Backward mode detection of laser-induced wide-band ultrasonic transients with optoacoustic transducer*. Journal of Applied Physics, 2000. **87**(4): p. 2003-2014.
19. Wang, T., P.D. Kumavor, and Q. Zhu, *Application of laser pulse stretching scheme for efficiently delivering laser energy in photoacoustic imaging*. J Biomed Opt, 2012. **17**(6): p. 061218.
20. Hu, S. and L.V. Wang, *Optical-resolution photoacoustic microscopy: auscultation of biological systems at the cellular level*. Biophysical journal, 2013. **105**(4): p. 841-847.
21. Wang, T., et al., *A low-cost photoacoustic microscopy system with a laser diode excitation*. Biomed Opt Express, 2014. **5**(9): p. 3053-8.
22. Yao, J., et al., *Photoimprint photoacoustic microscopy for three-dimensional label-free subdiffraction imaging*. Physical review letters, 2014. **112**(1): p. 014302.
23. Yao, J. and L.V. Wang, *Photoacoustic Microscopy*. Laser Photon Rev, 2013. **7**(5).
24. Lee, C.H., et al., *Near-Infrared Mesoporous Silica Nanoparticles for Optical Imaging: Characterization and In Vivo Biodistribution*. Advanced Functional Materials, 2009. **19**(2): p. 215-222.
25. Nie, L., et al., *Photoacoustic tomography through a whole adult human skull with a photon recycler*. Journal of biomedical optics, 2012. **17**(11): p. 110506-110506.
26. Nie, L., Z. Guo, and L.V. Wang, *Photoacoustic tomography of monkey brain using virtual point ultrasonic transducers*. Journal of biomedical optics, 2011. **16**(7): p. 076005-076005-5.

27. Erfanzadeh, M., et al. *Improvement and evaluation of a low-cost laser diode photoacoustic microscopy system for ovarian tissue imaging*. in *Proc. of SPIE Vol.* 2016.
28. Hariri, A., et al. *Low cost photoacoustic spectroscopy system for evaluation of skin health*. in *SPIE Optical Engineering+ Applications*. 2016. International Society for Optics and Photonics.
29. Roth, K., et al., *Imaging of a linear diode bar for an optical cell stretcher*. Biomedical optics express, 2015. **6**(3): p. 807-814.
30. Hu, S., K. Maslov, and L.V. Wang, *In vivo functional chronic imaging of a small animal model using optical-resolution photoacoustic microscopy*. Med Phys, 2009. **36**(6): p. 2320-3.
31. Maslov, K., et al., *Optical-resolution photoacoustic microscopy for in vivo imaging of single capillaries*. Opt Lett, 2008. **33**(9): p. 929-31.
32. Kharine, A., et al., *Poly (vinyl alcohol) gels for use as tissue phantoms in photoacoustic mammography*. Physics in medicine and biology, 2003. **48**(3): p. 357.
33. Reyes, D.K., et al., *Single-center phase II trial of transarterial chemoembolization with drug-eluting beads for patients with unresectable hepatocellular carcinoma: initial experience in the United States*. Cancer journal (Sudbury, Mass.), 2009. **15**(6): p. 526.
34. Zhang, C., et al., *Label-free photoacoustic microscopy of myocardial sheet architecture*. Journal of biomedical optics, 2012. **17**(6): p. 0605061-0605063.
35. Zhang, C., et al., *Label-free photoacoustic microscopy of cytochromes*. Journal of biomedical optics, 2013. **18**(2): p. 020504-020504.
36. Yuan, Y., S. Yang, and D. Xing, *Optical-resolution photoacoustic microscopy based on two-dimensional scanning galvanometer*. Applied Physics Letters, 2012. **100**(2): p. 023702.
37. Allen, T.J. and P.C. Beard, *Pulsed near-infrared laser diode excitation system for biomedical photoacoustic imaging*. Optics letters, 2006. **31**(23): p. 3462-3464.

Acknowledgement

I would like to express my deepest gratitude to my adviser Dr. Junghwan Oh, the professor of Department of Interdisciplinary program of Biomedical Mechanical & Electrical Engineering at Pukyong National University, for his invaluable guidance, support and encouragement toward the completion of the research and writing of this thesis. I have learned the principle knowledge of the photoacoustic from him. Dr. Oh will continue helping me to Biomedical Engineering research in PhD course.

I would also like to thank all my schoolmates and friends from my lab, Dr. Yun-ok Oh, Mr. Han-su Suh, Dr. Sudip, Dr. Santha, Dr. Mani, Dr. Raja, Quang, Bian, Vy, Phuoc, Nam, Phong, Hye Hyun and Jeayeop. They have helped me a lot with my research and always have been such good friends. Also, I am grateful to my parents and my beloved for their unending love, support and encouragement during two year of master.